1

Melting of Fe Alloys and the Thermal Structure of the Core

Rebecca A. Fischer

ABSTRACT

The temperature of the Earth's core has significant implications in many areas of geophysics, including applications to Earth's heat flow, core composition, age of the inner core, and energetics of the geodynamo. The temperature of the core at the inner core boundary is equal to the melting temperature of the core's Fe-rich alloy at the inner core boundary pressure. This chapter is a review of experimental results on melting temperatures of iron and Fe-rich alloys at core conditions that can thus be used to infer core temperatures. Large discrepancies exist between published melting curves for pure iron at high pressures, with better agreement on the melting behavior of Fe-light element alloys. The addition of silicon causes a small melting point depression in iron, while oxygen and especially sulfur cause larger melting point depressions. The inner core boundary temperature likely falls in the range 5150–6200 K, depending on the identity of the light element(s) in the core, which leads to a core-mantle boundary temperature of 3850–4600 K for an adiabatic outer core. The most significant sources of uncertainties in the core's thermal structure include the core's composition, phase diagram, and Grüneisen parameter.

1.1. INTRODUCTION

The Earth's core consists primarily of iron-nickel alloy. The presence of several weight percent of one or more lighter elements such as S, Si, O, C, or H is implied by the core's density, and these light elements depress the melting point of the core relative to pure iron [e.g., *Birch*, 1952; *Poirier*, 1994]. The thermal structure of the core plays a key role in many deep Earth properties. It affects the magnitude of the temperature difference across the thermal boundary layer at the base of the mantle, heat flow on Earth, and the cooling rate of the core. Faster cooling rates would imply a younger inner core, while slower cooling would imply an older inner core. The age of the inner core corresponds to the onset of compositional convection in the outer core due to the preferential expulsion of light elements during inner core crystallization. The core's temperature structure is also linked to thermal convection in the outer core, with these two types of convection driving the dynamo responsible for Earth's magnetic field [e.g., *Lister and Buffett*, 1995]. The vigor of thermal convection in the Earth's core depends on both its thermal structure and its thermal conductivity. Recent studies on the thermal conductivity of Fe and Fe-rich alloys at core conditions have revealed a higher thermal conductivity of core materials than previously thought [e.g., *Pozzo et al.*, 2012; *Seagle et al.*, 2013], implying that higher core temperatures and/or stronger compositional convection are required to power the dynamo.

Knowledge of the core's temperature would inform our understanding of these processes and put tighter constraints

Department of the Geophysical Sciences, University of Chicago, Chicago, Illinois, USA

Deep Earth: Physics and Chemistry of the Lower Mantle and Core, *Geophysical Monograph 217*, First Edition.
Edited by Hidenori Terasaki and Rebecca A. Fischer.

on the abundances of light elements in the Earth's core, since thermal expansion affects the quantity of light elements needed to match the observed density. The temperature at the inner core boundary (ICB) is equal to the liquidus temperature of the core alloy at that pressure (~330 GPa), since that is the temperature at which the solid inner core is crystallizing from the liquid outer core. Therefore knowledge of the ICB temperature could be combined with measurements of phase diagrams at high pressures and temperatures (P and T) to constrain the identities of the core's light elements. However, the thermal structure of the core is poorly understood.

This chapter reviews the available experimental constraints on the core's temperature. Measuring melting of iron and Fe-rich alloys at core conditions presents significant experimental challenges, leading to discrepancies between studies. Extrapolating melting curves to the ICB pressure provides information about the ICB temperature. Adiabats can be calculated through these P-T points up to the core-mantle boundary (CMB) pressure to determine the thermal structure of the outer core.

1.2. METHODS FOR DETERMINATION OF MELTING

Melting experiments relevant to the Earth's core require the generation of simultaneous extreme pressures and temperatures. This is commonly accomplished through the use of a laser-heated diamond anvil cell, which is capable of reaching inner core conditions. A sample is embedded in a soft, inert pressure-transmitting medium and compressed between two diamond anvils, then heated with an infrared laser until melted. Pressure is typically monitored using an X-ray standard in the sample chamber whose equation of state is well known or by ruby fluorescence or diamond Raman spectroscopy, whose signals shift systematically with pressure. Temperature is measured spectroradiometrically by fitting the thermal emission to the Planck function (see *Salamat et al.* [2014] for a recent review of diamond anvil cell methodology).

While techniques for generating and measuring extreme P-T conditions in the diamond anvil cell are relatively well established, there is disagreement over the best method for detecting a melt signal. Some studies rely on "speckling," a qualitative detection of movement in the sample visualized by shining a second (visible) laser onto the laser-heated spot during the experiment [e.g., *Boehler*, 1993]. This movement is thought to be due to convection of the molten sample, though it has recently been proposed that rapid recrystallization of the sample at subsolidus conditions can cause this apparent motion [*Anzellini et al.*, 2013; *Lord et al.*, 2014a]. Other methods rely on discontinuities in physical properties upon melting, such as a change in the emissivity-temperature relationship [*Campbell*, 2008; *Fischer and Campbell*, 2010] or in the laser power-temperature relationship [e.g., *Lord et al.*, 2009]. These methods have the advantage of not requiring a synchrotron X-ray source but provide no structural information about subsolidus phases. Synchrotron-based techniques include the use of X-ray diffraction to detect diffuse scattering from the melt and/or disappearance of crystalline diffraction [e.g., *Anzellini et al.*, 2013; *Campbell et al.*, 2007; *Fischer et al.*, 2012, 2013] or, less commonly, time domain synchrotron Mössbauer spectroscopy [*Jackson et al.*, 2013].

In addition to diamond anvil cell methods, the multianvil press has also been used for melting experiments, with analysis of recovered samples used to detect melting [e.g., *Fei and Brosh*, 2014; *Fei et al.*, 2000]. Previously multianvil press experiments were limited in pressure to ~25 GPa, but recent advances in sintered diamond anvils [e.g., *Yamazaki et al.*, 2012] may allow for higher-pressure melting experiments in the multianvil press in the future. Until recently, shock wave experiments were the standard technique for melting experiments at core conditions [e.g., *Brown and McQueen*, 1986]. They provide a reliable method for reaching core pressures and temperatures, with melting determined from discontinuities in the sound velocity-pressure relationship. However, temperatures in shock experiments are frequently calculated thermodynamically [e.g., *Brown and McQueen*, 1986; *Nguyen and Holmes*, 2004] due to difficulties with direct measurements, making them less accurate, and improvements in diamond cell methods have facilitated the access of core conditions by static methods. Additionally, melting curves can be calculated using ab initio methods [e.g., *Alfè et al.*, 2002] or thermodynamic modeling [e.g., *Fei and Brosh*, 2014].

1.3. RESULTS ON MELTING OF IRON

Due to its extreme importance to our understanding of the thermal structure of the core, the melting behavior of iron at high pressures has been investigated by many research groups using all of the techniques discussed in Section 1.2. Despite such a large number of results using a variety of methods, there remains no consensus on the melting curve of pure iron at core pressures. Figure 1.1 illustrates some of the many previous results on iron melting obtained using diamond anvil cell [*Anzellini et al.*, 2013; *Boehler*, 1993; *Jackson et al.*, 2013; *Ma et al.*, 2004; *Saxena et al.*, 1994; *Shen et al.*, 2004; *Williams et al.*, 1987], ab initio [*Alfè*, 2009; *Alfè et al.*, 2002; *Anderson et al.*, 2003; *Belonoshko et al.*, 2000; *Laio et al.*, 2000; *Sola and Alfè*, 2009], and shock wave [*Ahrens et al.*, 2002; *Brown and McQueen*, 1986; *Nguyen and Holmes*, 2004; *Yoo et al.*, 1993] methods. Below ~50 GPa there is fairly good agreement over the iron melting curve. In the ~50–200 GPa range, readily accessible in the laser-heated diamond anvil

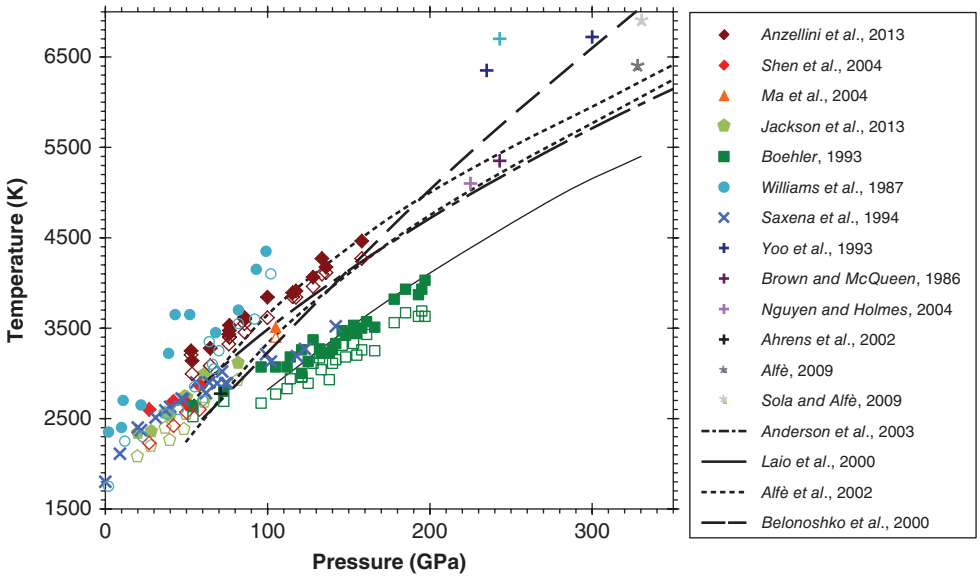

Figure 1.1 Selection of the literature results on Fe melting illustrating range of discrepancy in the literature. Open symbols are lower bounds; filled symbols are upper bounds. Symbols are color coded by study (e.g., teal circles and + symbols are all from *Williams et al.* [1987]), with shape indicating the method used to detect melting. Diamonds: X-ray diffuse scattering. Triangles: loss of X-ray signal. Pentagons: Mössbauer spectroscopy. Squares: visual observation of motion ("speckling"). Circles: changes in sample appearance. × symbols: discontinuity in laser power-temperature relationship. + symbols: shock wave methods. Curves and * symbols: ab initio methods. The lower and upper curves of *Alfè et al.* [2002] were calculated with and without free energy corrections, respectively.

cell, Fe melting curves vary by over 1000 K. Where the shock Hugoniot crosses the melting curve at ~240 GPa, reported shock melting temperatures vary by ~1500 K. At the inner core boundary pressure of 330 GPa, ab initio calculations of Fe melting vary by over 1500 K.

The causes of these discrepancies remain unclear. Among diamond anvil cell studies, it appears that the method used to detect melting is one of the main sources of variation [e.g., *Anzellini et al.*, 2013; *Jackson et al.*, 2013], though there is no clear consensus as to which method should be the most reliable. Uncertainties in radiometric temperature measurements, pressure calibrations, and possible chemical reactions at these extreme conditions may also play a role in the discrepancy. Among shock wave experiments, large uncertainties in temperature determination may explain some of the variability [e.g., *Brown and McQueen*, 1986]. A systematic offset is seen between shock studies in which temperatures are calculated thermodynamically [*Brown and McQueen*, 1986; *Nguyen and Holmes*, 2004] and those in which they are measured spectroradiometrically [*Williams et al.*, 1987; *Yoo et al.*, 1993] (Figure 1.1). Studies in which temperatures are calculated thermodynamically give systematically lower melting temperatures, in better agreement with the static diamond anvil cell results.

The melting point of iron at 330 GPa may be taken as an upper bound on the temperature at the inner core boundary, neglecting the effects of an alloying light element. However, the experimental studies represented in Figure 1.1 reported ICB temperatures ranging from 4850 K [*Boehler*, 1993] to 7600 K [*Williams et al.*, 1987]. *Anzellini et al.* [2013] suggested that earlier diamond cell studies that identified melting at lower temperatures may have actually been identifying the onset of fast recrystallization. The authors point to the agreement between several more recent studies (diffuse scattering results of *Anzellini et al.* [2013], some shock wave studies [*Brown and McQueen*, 1986; *Nguyen and Holmes*, 2004], and some ab initio studies [e.g., *Alfè*, 2009; *Alfè et al.*, 2002]) as evidence of progress toward a consensus on the Fe melting curve. Additionally, coincidence of fast recrystallization with melting temperatures reported using the speckling technique was also reported by *Lord et al.* [2014a] on a different material. Therefore, in this discussion, the melting curve of *Anzellini et al.* [2013] will be used as the reference for pure iron, though uncertainties remain. For example, lower melting temperatures for iron were reported by other shock wave [*Ahrens et al.*, 2002] and diamond cell studies, including those using identical melting criteria [*Shen et al.*, 2004]. Despite decades of effort to measure the melting curve of iron, further work remains necessary.

1.4. RESULTS ON MELTING OF IRON-RICH ALLOYS

The core's density implies the presence of several weight percent of one or more light elements [e.g., *Birch*, 1952], which lowers the melting point of iron. Therefore it is important to consider the effects of these light elements on the melting of iron at core conditions. Surprisingly, the eutectic melting behavior in more complex multicomponent systems involving iron and one or more light elements is often more well-understood than the end-member case.

Melting in Fe-rich iron-silicon alloys has been the subject of several previous studies using X-ray diffuse scattering [*Fischer et al.*, 2012, 2013; *Morard et al.*, 2011], laser power-temperature discontinuities [*Asanuma et al.*, 2010; *Fischer et al.*, 2013], and morphology of recovered samples [*Asanuma et al.*, 2010]. Figure 1.2a illustrates melting results in the Fe-FeSi system on compositions ranging from 9 to 18 wt % Si up to 140 GPa. Since the addition of this amount of silicon must depress the melting point of iron, the melting results in Figure 1.2a lend support to the higher reported melting curves of pure Fe [i.e., *Anzellini et al.*, 2013; *Williams et al.*, 1987]. Taking the Fe melting curve of *Anzellini et al.* [2013] as a reference, the addition of Si causes a melting point depression of approximately 0–400 K at 100 GPa. At higher pressures than this, the eutectic temperature appears to stop increasing with pressure, but there are very few Fe-Si melting data at these conditions. This pressure approximately corresponds to a transition from a face-centered-cubic (fcc) + B2 to a hexagonal close-packed (hcp) + B2 subsolidus phase assemblage [*Fischer et al.*, 2013], which may explain the change in slope of the eutectic temperature with increasing pressure. This behavior could imply that the melting point depression caused by silicon increases at higher pressures; however, additional melting data on Fe-Si alloys at higher pressures are needed to clarify this. The scatter in Figure 1.2a is due in part to changes in the subsolidus phase assemblage being melted, which may be fcc + B2, hcp + B2, DO_3 only, or B2 only below ~100 GPa, depending on pressure and composition. However, all compositions shown in Figure 1.2a should melt eutectically from an hcp + B2 mixture above ~100 GPa [*Fischer et al.*, 2013].

Figure 1.2b summarizes melting results in the Fe-FeO system obtained using the "speckle" method [*Boehler*, 1993] and the disappearance of crystalline X-ray diffraction peaks [*Seagle et al.*, 2008] as melting criteria up to 140 GPa. The data of *Seagle et al.* [2008] and *Boehler* [1993] are compatible within uncertainty. It is interesting to note that these two different melting criteria indicate approximately the same melting temperatures in the Fe-FeO system, while they give very different results on pure Fe (Section 1.3). Oxygen causes a deeper melting point depression in iron than silicon does. At 100 GPa, the experimental results shown in Figure 1.2b demonstrate that the Fe-FeO eutectic temperature is approximately 700–1100 K lower than the Fe melting curve of *Anzellini et al.* [2013]. Thermodynamic calculations of *Komabayashi* [2014] using an ideal solution model for the Fe-FeO eutectic are compatible with the upper end of this range. Changes in the subsolidus crystal structure of FeO at higher pressures [*Ozawa et al.*, 2011] could change the melting behavior, but melting data in the Fe-FeO system are not yet available at these conditions (P> 240 GPa).

Previous results on the Fe-Fe_3S melting curve exhibit a remarkable degree of agreement between studies that used a variety of different melting criteria. Figure 1.2c shows some of these results, in which melting was determined from the disappearance of crystalline X-ray diffraction [*Campbell et al.*, 2007; *Kamada et al.*, 2012], the appearance of diffuse X-ray scattering [*Morard et al.*, 2008, 2011], and scanning electron microscope observations of recovered samples [*Chudinovskikh and Boehler*, 2007]. From 21 to ~240 GPa in the Fe-rich side of the Fe-S system, the subsolidus phase assemblage is a mixture of Fe and Fe_3S [*Fei et al.*, 2000; *Kamada et al.*, 2010], though Fe_3S decomposition at higher pressures could change the slope of the melting curve [*Ozawa et al.*, 2013]. The Fe-Fe_3S melting curve shows a small change in slope at ~60 GPa, where the fcc-hcp phase boundary in iron intersects the Fe-Fe_3S melting curve [*Morard et al.*, 2011]; effects of this transition are not well resolved in the Fe-FeO system, likely due to scatter in the data. Eutectic melting in the Fe-Fe_3S system occurs ~900–1200 K lower than the melting point of iron [*Anzellini et al.*, 2013] at 100 GPa.

Melting in the Fe-Fe_3C system was investigated by *Lord et al.* [2009] to 70 GPa using the laser power-temperature discontinuity method and X-ray radiography (Figure 1.2d). New multianvil press experiments and calculations in the Fe-C system by *Fei and Brosh* [2014] have reproduced the Fe-Fe_3C eutectic melting curve of *Lord et al.* [2009]. The Fe-Fe_3C eutectic is 600–800 K lower than the Fe melting curve of *Anzellini et al.* [2013] at 70 GPa. The Fe-Fe_3C melting curve has approximately the same slope as the Fe melting curve of *Anzellini et al.* [2013] at these pressures, so the melting point depression at 100 GPa is also expected to be ~600–800 K. It is likely that Fe_7C_3 will replace Fe_3C as the stable carbide along the eutectic at core conditions [*Fei and Brosh*, 2014; *Lord et al.*, 2009], which could change the melting behavior in this system at higher pressures. Carbon in the core is discussed further in Chapter 22.

Melting in the Fe-H system has not been studied nearly as thoroughly as other Fe-light element systems, due at least in part to technical challenges. It has only been studied up to 20 GPa [*Sakamaki et al.*, 2009] and only in the presence of excess H, which is likely a different

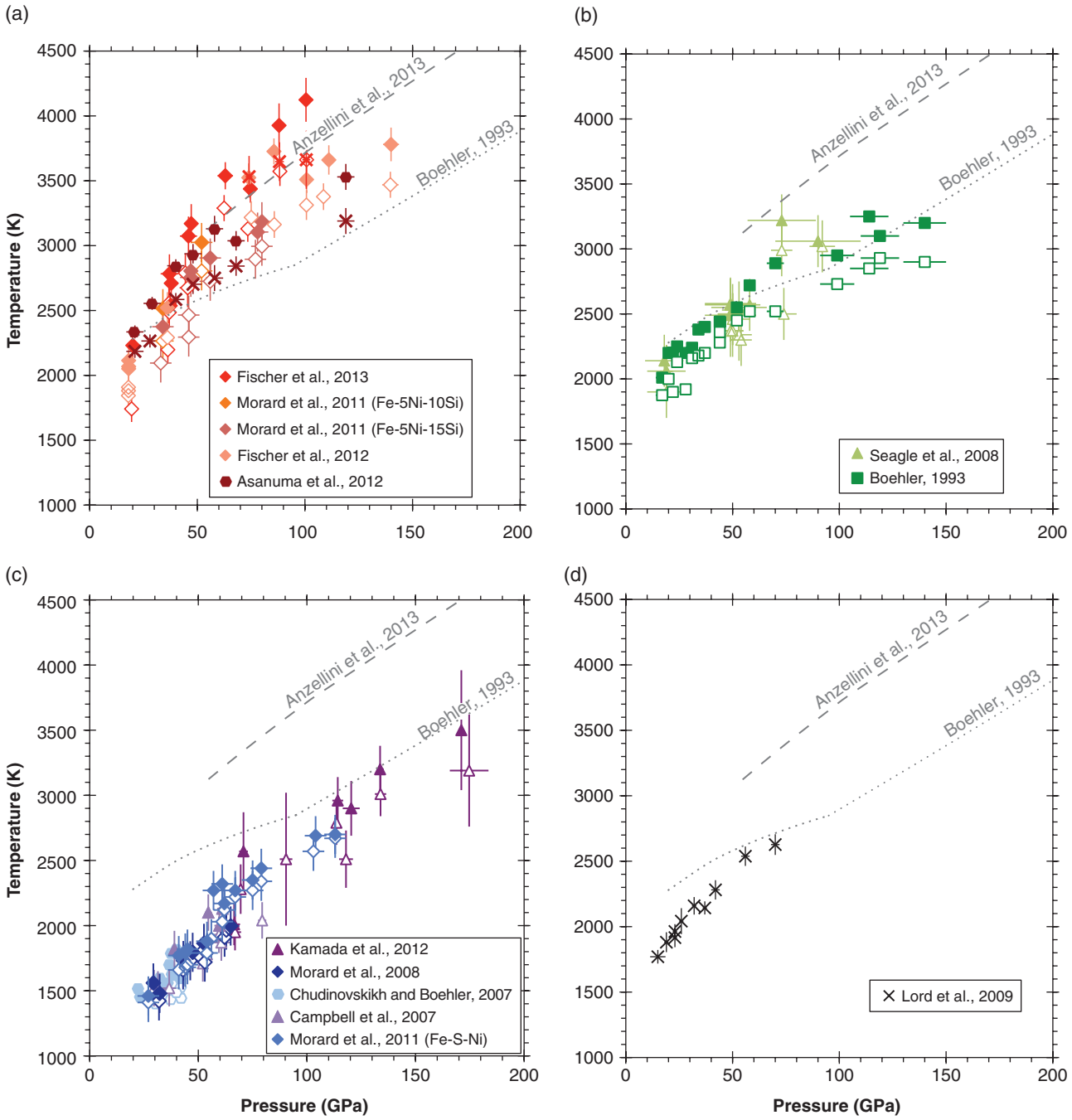

Figure 1.2 Solidus temperatures in (a) Fe-FeSi, (b) Fe-FeO, (c) Fe-Fe_3S, and (d) Fe-Fe_3C binary systems (some data also contain Ni). Open symbols (and × symbols from *Asanuma et al.* [2010]) are lower bounds; filled symbols are upper bounds. Dashed and dotted grey lines show high and low melting curves for pure Fe for comparison. Symbols are color coded by study, with shape indicating the method used to detect melting. Hexagons: scanning electron microscope imaging of recovered sample texture. Other symbol shapes are as in Figure 1.1.

eutectic from that relevant to the Earth's core composition. Other aspects of hydrogen in the core are reviewed in Chapter 20.

Melting in ternary systems has not been extensively studied at core pressures. *Terasaki et al.* [2011] and *Huang et al.* [2010] measured melting on Fe-rich compositions in the Fe-O-S system using static and shock methods, respectively. *Terasaki et al.* [2011] report a eutectic melting point depression of ~950–1200 K relative to the Fe melting curve of *Anzellini et al.* [2013] at 100 GPa,

indistinguishable from results on the Fe-S system without oxygen present. *Huang et al.* [2010] report a smaller melting point depression of 300–800 K, which is incompatible with results on Fe-S and Fe-O melting, since the addition of a small amount of a second light element is unlikely to increase the melting point.

Nickel has only a minor effect on the melting temperatures of iron-light element alloys, though many of the data on the effects of nickel were obtained far below core pressures. Comparing the melting data of *Morard et al.* [2011] on Fe-Si-Ni alloys to results without nickel (Figure 1.2a) reveals no resolvable effect of 5% Ni on the melting temperature, though this is difficult to assess given the scatter in the Fe-Si(-Ni) data. *Lord et al.* [2014b] reported similar melting temperatures of Fe-Si-Ni alloys. The shock wave study of *Zhang et al.* [2014] reported melting temperatures for Fe-9Ni-10Si at 168 and 206 GPa that are compatible with the Ni-free data in Figure 1.2a. *Zhang and Fei* [2008] investigated the Fe-S-Ni system at ~20 GPa and found that the addition of 5% Ni lowers the melting point by 50–100 K, compatible with the findings of *Stewart et al.* [2007]. *Morard et al.* [2011] found no resolvable effect of 5% Ni in an Fe-S-Ni alloy at higher pressures (Figure 1.2c). *Urakawa et al.* [1987] reported a 100 K melting point depression from the addition of 10% Ni to the Fe-O-S system at 6–15 GPa. *Rohrbach et al.* [2014] found an ~50 K melting point depression when 5% Ni is added to the Fe-C system at 10 GPa. New results on the melting of pure Ni [*Lord et al.*, 2014a] show that its melting curve is very similar to the melting curve of pure Fe reported by *Anzellini et al.* [2013], as opposed to being significantly lower as previously thought, so a deep melting point depression is not required.

1.5. APPLICATION TO THE THERMAL STRUCTURE OF THE CORE

Eutectic melting point depressions caused by different light elements at 100 GPa relative to the Fe melting curve of *Anzellini et al.* [2013] (Section 1.4) are summarized in Table 1.1. They can be used to extrapolate the melting curves of these Fe-light element alloys to the inner core boundary pressure by subtracting this depression from the melting curve of iron, which has been determined to higher pressures and thus requires less extrapolation. Extrapolation of these melting curves assumes that any subsolidus phase changes at higher pressures do not significantly affect the slopes of the melting curves, which is necessary given the pressure ranges of the data. *Anzellini et al.* [2013] report a melting temperature of pure iron of 6200 ± 500 K at 330 GPa based on an extrapolation of their data, which are compatible with the shock data of *Nguyen and Holmes* [2004] and *Brown and McQueen* [1986] and the ab initio study of *Alfè* [2009]. The uncertainties involved are likely larger than this, based on the disagreement between studies at lower pressures (Figure 1.1) and uncertainties inherent in this extrapolation. The melting temperatures at 330 GPa for different binary systems can be calculated by assuming that melting point depressions at 100 GPa can approximate those at 330 GPa. These results are listed in Table 1.1. Since the melting temperatures are compared to the same melting curve of Fe at both 100 and 330 GPa, the melting temperatures listed in Table 1.1 are approximately independent of the choice of Fe melting curve if the melting curves have similar slopes. However, the melting point depressions reported in Table 1.1 do depend on the choice of Fe melting curve.

Table 1.1 Melting point depressions at 100 GPa (relative to the Fe melting curve of *Anzellini et al.* [2013]) and estimated 330 GPa eutectic melting temperatures for various iron-light element binary systems.

System	Melting point depression (K)	Melting temperature at ICB (K)
Fe	0	6200 ± 500
Fe-Si	0–400	6000 ± 500
Fe-O	700–1100	5300 ± 500
Fe-S	900–1200	5150 ± 500
Fe-C	600–800	5500 ± 500

These results can be compared to a simple extrapolation of the data obtained by fitting the Simon equation to all of the data shown in Figure 1.2 for each composition. However, these fits are very sensitive to the choice of the reference pressure and temperature, which is a large source of uncertainty. Upper and lower bounds were fit separately, resulting in a range of melting temperatures (except in the Fe-C system). This method predicts melting temperatures at 330 GPa of 5250–5600 K (Fe-Si), 4200–4650 K (Fe-O), 4500–5300 K (Fe-S), and 5100 K (Fe-C). These values are generally lower than those listed in Table 1.1 but compatible within uncertainty. The exception is the Fe-O system, in which the data from *Boehler* [1993] imply a significantly shallower slope than the melting curve of *Anzellini et al.* [2013] (though the more recent data of *Seagle et al.* [2008] do not), resulting in a lower melting temperature when extrapolated directly.

It is important to note that the melting temperatures at 330 GPa listed in Table 1.1 are eutectic temperatures. Therefore, they represent lower bounds on Earth's inner core boundary temperature, since the inner core is crystallizing from the liquid outer core along the liquidus, not at the eutectic temperature. Improved understanding of how the liquidus temperature evolves with pressure, temperature, and composition in these systems would produce a better estimate of the ICB temperature. However, the presence of significant quantities of multiple light elements in the core could decrease the melting temperature relative to those of binary systems.

In this discussion the eutectic melting temperatures of the binary Fe-light element alloys listed in Table 1.1 are taken as approximations of the ICB temperature.

These melting temperatures (Table 1.1) therefore represent points to which the core's geotherm may be anchored at 330 GPa for different compositions. The inner core is believed to be relatively isothermal, with a uniform temperature to within ~100 K [*Brown and Shankland*, 1981; *Pozzo et al.*, 2014]. The convecting outer core is mostly adiabatic [e.g., *Birch*, 1952]. Thermally stratified layers have been suggested based on recent calculations of high thermal conductivity of Fe [*Pozzo et al.*, 2012], though thermal conductivity is compositionally dependent [*Seagle et al.*, 2013]. In particular, a thermochemical boundary layer at the base of the outer core [e.g., *Gubbins et al.*, 2008] and a stratified layer at the top of the outer core [e.g., *Buffett*, 2014] have both been proposed, with the bulk of the outer core considered to be adiabatic. The magnitude of possible deviations from adiabaticity is poorly constrained.

Assuming that the temperature gradient in the outer core can be approximated as adiabatic, its temperature profile may be calculated from

$$\gamma(\rho) = \frac{\partial \ln T}{\partial \ln \rho},$$

where γ is the Grüneisen parameter, a function of density ρ. Different equations of state will therefore produce core adiabats with different slopes. Equations of state of possible core components are reviewed in Chapter 10. Here a recent thermal equation of state of hcp iron [*Dewaele et al.*, 2006] is taken as representative of Fe-rich alloys for geotherm calculations. Using the thermal equation-of-state parameters for iron from *Anderson* [1998], for example, would change the temperature at 135 GPa by ~250 K. This calculation is primarily sensitive to the value of the Grüneisen parameter at core conditions and less sensitive to the Debye temperature and isothermal equation-of-state parameters, such as the bulk modulus, its pressure derivative, and the density at 1 bar.

Figure 1.3 illustrates some example core adiabats anchored to the 330 GPa melting points of each binary system listed in Table 1.1. Inner core boundary temperatures of 5150–6200 K translate into core-mantle boundary temperatures of 3850–4600 K along an adiabat. Extrapolating transition zone temperatures along an adiabat to the core-mantle boundary predicts a mantle temperature of 2500–2800 K approaching the CMB [*Lay et al.*, 2008], implying a temperature contrast across the thermal boundary layer of 1050–2100 K. Assuming a mantle thermal conductivity of 10 W/m·K in a 200-km-thick thermal boundary layer [*Lay et al.*, 2008], this temperature contrast leads to a heat flux q of 0.05–0.11 W/m^2, corresponding to a heat flow of 8–15 TW. Only the highest end of this range (corresponding to the highest core temperature) is compatible with recent calculations of

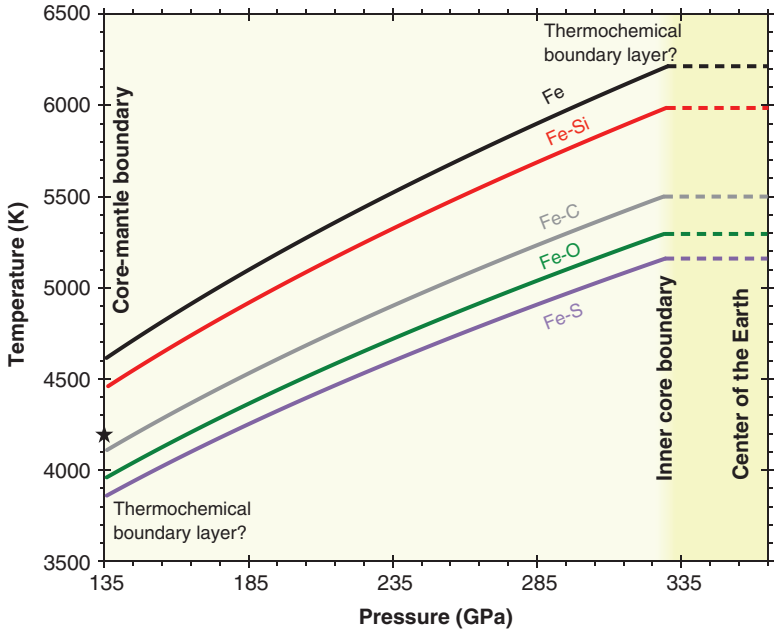

Figure 1.3 Thermal structure of the core for different core compositions. Outer core adiabats are calculated from the equation of state of Fe [*Dewaele et al.*, 2006] and anchored to 330 GPa melting points for pure Fe and Fe-Si, Fe-C, Fe-O, and Fe-S binary systems (Table 1.1). Small departures from adiabaticity may occur at the top and bottom of the outer core. The inner core is approximated as isothermal. Black star at 135 GPa is the mantle solidus [*Andrault et al.*, 2011; *Fiquet et al.*, 2010].

the core's thermal conductivity [e.g., *Pozzo et al.*, 2012], though experiments have shown that iron's thermal conductivity has a significant compositional dependence [*Seagle et al.*, 2013]. Based on estimates of the degree of partial melt at the base of the mantle, which range from zero to ~25% [e.g., *Rost et al.*, 2005], these high temperatures may be incompatible with measurements of mantle melting temperatures, though there are discrepancies between studies. Reported mantle solidus temperatures range from 3600 K [*Nomura et al.*, 2014] to 4200 K [*Andrault et al.*, 2011; *Fiquet et al.*, 2010] at 135 GPa (Figure 1.3), with liquidus temperatures ranging from 4700 K [*Andrault et al.*, 2011] to ~5400 K [*Fiquet et al.*, 2010].

An Fe-Si core implies the highest core temperatures, followed by Fe-C, then Fe-O, with an Fe-S core implying the lowest temperatures. The small difference between the melting curves of pure Fe and Fe-Si (Figure 1.2a) suggests a narrow phase loop between the solidus and liquidus in the Fe-Si system, so that an Fe-Si core would likely drive compositional convection less efficiently than an Fe-O or Fe-S core would. An Fe-Si core may therefore require a larger thermal convection contribution to maintain the geodynamo relative to an Fe-O or Fe-S core. The width of this phase loop between the solidus and liquidus must be compatible with the density contrast between the inner and outer core, offering another clue into the identity of the core's light element(s). The Fe-Si melting curve is steeper than those of Fe-O and Fe-S (Figure 1.2). This implies that for a given core cooling rate an Fe-Si core would crystallize more slowly than an Fe-O or Fe-S core would [*Fischer et al.*, 2013]. Therefore, a core with silicon as the dominant light element would have an older inner core than one rich in oxygen or sulfur, implying an earlier onset of compositional convection if silicon is the dominant light element.

1.6. CONCLUSIONS

Geotherms in the Earth's outer core can be calculated as an adiabat if the melting temperature of the core alloy at 330 GPa and its equation of state are known. The temperature in Earth's outer core likely ranges from 3850–4600 K at the CMB to 5150–6200 K at the ICB, but large uncertainties remain. Despite decades of research and its significance in geophysics, controversy still surrounds the melting temperature of pure iron at Earth's core conditions, though a consensus may be starting to form. However, the pressure evolution of eutectic temperatures in the Fe-Si, Fe-O, and Fe-S systems is better understood, largely due to the development of synchrotron X-ray diffraction techniques for in situ detection of melting. Silicon causes a small melting point depression in iron, while oxygen and sulfur cause larger melting point depressions, with implications for the core's evolution. For example, an Fe-Si core would drive compositional convection less efficiently and crystallize more slowly than an Fe-O or Fe-S core. Knowledge of these melting curves, combined with information about densities, seismic velocities, solid-melt partitioning, geochemistry, and other independent constraints on properties of various light element candidates (as discussed in Parts II–V of this monograph), offers clues to the core's composition.

Future studies aiming to further our understanding of the temperature of the core should focus on how melting temperatures of Fe-rich systems vary with pressure and composition, especially in ternary systems, and on the Grüneisen parameters of (liquid) Fe-rich alloys at core conditions. It is especially important to focus on measurements of liquidus temperatures since the inner core is crystallizing along the liquidus. Melting measurements are needed at higher pressures, both to reduce uncertainties inherent in extrapolations and to identify the effects of subsolidus phase changes on melting.

ACKNOWLEDGMENTS

I thank Andrew J. Campbell for helpful discussions, editor Hidenori Terasaki for handling this manuscript, and two anonymous reviewers for constructive comments. This work was supported by an American Dissertation Fellowship from the American Association for University Women to R.A.F. and by the National Science Foundation grant EAR-1427123 to A.J.C.

REFERENCES

Ahrens, T. J., K. G. Holland, and G. Q. Chen (2002), Phase diagram of iron, revised-core temperatures, *Geophys. Res. Lett.*, *29*, 1150, doi:10.1029/2001GL014350.

Alfè, D. (2009), Temperature of the inner-core boundary of the Earth: Melting of iron at high pressure from first-principles coexistence simulations, *Phys. Rev. B*, *79*, 060101, doi:10.1103/PhysRevB.79.060101.

Alfè, D., G. D. Price, and M. J. Gillan (2002), Iron under Earth's core conditions: Liquid-state thermodynamics and high-pressure melting curve from *ab initio* calculations, *Phys. Rev. B*, *65*, 165 118, doi:10.1103/PhysRevB.65.165118.

Anderson, O. L. (1998), The Grüneisen parameter for iron at outer core conditions and the resulting conductive heat and power in the core, *Phys. Earth Planet. Inter.*, *109*, 179–197, doi:10.1016/S0031-9201(98)00123-X.

Anderson, O. L., D. G. Isaak, and V. E. Nelson (2003), The high-pressure melting temperature of hexagonal close-packed iron determined from thermal physics, *J. Phys. Chem. Solids*, *64*, 2125–2131, doi:10.1016/S0022-3697(03)00112-4.

Andrault, D., N. Bolfan-Casanova, G. Lo Nigro, M. A. Bouhifd, G. Garbarino, and M. Mezouar (2011), Solidus and liquidus profiles of chondritic mantle: Implication for melting

of the Earth across its history, *Earth Planet. Sci. Lett.*, *304*, 251–259, doi:10.1016/j.epsl.2011.02.006.

Anzellini, S., A. Dewaele, M. Mezouar, P. Loubeyre, and G. Morard (2013), Melting of iron at Earth's inner core boundary based on fast X-ray diffraction, *Science*, *340*, 464–466, doi:10.1126/science.1233514.

Asanuma, H., E. Ohtani, T. Sakai, H. Terasaki, S. Kamada, T. Kondo, and T. Kikegawa (2010), Melting of iron–silicon alloy up to the core–mantle boundary pressure: Implications to the thermal structure of Earth's core, *Phys. Chem. Minerals*, *37*, 353–359, doi:10.1007/s00269-009-0338-7.

Belonoshko, A. B., R. Ahuja, and B. Johansson (2000), Quasi-*ab initio* molecular dynamic study of Fe melting, *Phys. Rev. Lett.*, *84*, 3638–3641, doi:10.1103/PhysRevLett.84.3638.

Birch, F. (1952), Elasticity and constitution of the Earth's interior, *J. Geophys. Res.*, *57*, 227–286, doi:10.1029/JZ057i002p00227.

Boehler, R. (1993), Temperatures in the Earth's core from melting-point measurements of iron at high static pressures, *Nature*, *363*, 534–536, doi:10.1038/363534a0.

Brown, J. M., and R. G. McQueen (1986), Phase transitions, Grüneisen parameter, and elasticity for shocked iron between 77 GPa and 400 GPa, *J. Geophys. Res.*, *91*, 7485–7494, doi:10.1029/JB091iB07p07485.

Brown, J. M., and T. J. Shankland (1981), Thermodynamic parameters in the Earth as determined from seismic profiles, *Geophys. J. R. Astron. Soc.*, *66*, 579–596, doi:10.1111/j.1365-246X.1981.tb04891.x.

Buffett, B. (2014), Geomagnetic fluctuations reveal stable stratification at the top of the Earth's core, *Nature*, *507*, 484–487, doi:10.1038/nature13122.

Campbell, A. J. (2008), Measurement of temperature distributions across laser heated samples by multispectral imaging radiometry, *Rev. Sci. Instrum.*, *79*, 015108, doi:10.1063/1.2827513.

Campbell, A. J., C. T. Seagle, D. L. Heinz, G. Shen, and V. B. Prakapenka (2007), Partial melting in the iron–sulfur system at high pressure: A synchrotron X-ray diffraction study, *Phys. Earth Planet. Inter.*, *162*, 119–128, doi:10.1016/j.pepi.2007.04.001.

Chudinovskikh, L., and R. Boehler (2007), Eutectic melting in the system Fe-S to 44 GPa, *Earth Planet. Sci. Lett.*, *257*, 97–103, doi:10.1016/j.epsl.2007.02.024.

Dewaele, A., P. Loubeyre, F. Occelli, M. Mezouar, P. I. Dorogokupets, and M. Torrent (2006), Quasihydrostatic equation of state of iron above 2 Mbar, *Phys. Rev. Lett.*, *97*, 215504, doi:10.1103/PhysRevLett.97.215504.

Fei, Y., and E. Brosh (2014), Experimental study and thermodynamic calculations of phase relations in the Fe–C system at high pressure, *Earth Planet. Sci. Lett.*, *408*, 155–162, doi:10.1016/j.epsl.2014.09.044.

Fei, Y., J. Li, C. M. Bertka, and C. T. Prewitt (2000), Structure type and bulk modulus of Fe_3S, a new iron-sulfur compound, *Am. Mineral.*, *85*, 1830–1833.

Fiquet, G., A. L. Auzende, J. Siebert, A. Corgne, H. Bureau, H. Ozawa, and G. Garbarino (2010), Melting of peridotite to 140 gigapascals, *Science*, *329*, 1516–1518, doi:10.1126/science.1192448.

Fischer, R. A., and A. J. Campbell (2010), High-pressure melting of wüstite, *Am. Mineral.*, *95*, 1473–1477, doi:10.2138/am.2010.3463.

Fischer, R. A., A. J. Campbell, R. Caracas, D. M. Reaman, P. Dera, and V. B. Prakapenka (2012), Equation of state and phase diagram of Fe–16Si alloy as a candidate component of Earth's core, *Earth Planet. Sci. Lett., 357–358*, 268–276, doi:10.1016/j.epsl.2012.09.022.

Fischer, R. A., A. J. Campbell, D. M. Reaman, N. A. Miller, D. L. Heinz, P. Dera, and V. B. Prakapenka (2013), Phase relations in the Fe–FeSi system at high pressures and temperatures, *Earth Planet. Sci. Lett.*, *373*, 54–64, doi:10.1016/j.epsl.2013.04.035.

Gubbins, D., G. Masters, and F. Nimmo (2008), A thermochemical boundary layer at the base of Earth's outer core and independent estimate of core heat flux, *Geophys. J. Int.*, *174*, 1007–1018, doi:10.1111/j.1365-246X.2008.03879.x.

Huang, H., X. Hu, F. Jing, L. Cai, Q. Shen, Z. Gong, and H. Liu (2010), Melting behavior of Fe–O–S at high pressure: A discussion on the melting depression induced by O and S, *J. Geophys. Res.*, *115*, B05207, doi:10.1019/2009JB006514.

Jackson, J. M., W. Sturhahn, M. Lerche, J. Zhao, T. S. Toellner, E. E. Alp, S. V. Sinogeikin, J. D. Bass, C. A. Murphy, and J. K. Wicks (2013), Melting of compressed iron by monitoring atomic dynamics, *Earth Planet. Sci. Lett.*, *362*, 143–150, doi:10.1016/j.epsl.2012.11.048.

Kamada, S., H. Terasaki, E. Ohtani, T. Sakai, T. Kikegawa, Y. Ohishi, N. Hirao, N. Sata, and T. Kondo (2010), Phase relationships of the Fe–FeS system in conditions up to the Earth's outer core, *Earth Planet. Sci. Lett.*, *294*, 94–100, doi:10.1016/j.epsl.2010.03.011.

Kamada, S., E. Ohtani, H. Terasaki, T. Sakai, M. Miyahara, Y. Ohishi, and N. Hirao (2012), Melting relationships in the Fe–Fe_3S system up to the outer core conditions, *Earth Planet. Sci. Lett., 359–360*, 26–33, doi:10.1016/j.epsl.2012.09.038.

Komabayashi, T. (2014), Thermodynamics of melting relations in the system Fe–FeO at high pressure: Implications for oxygen in the Earth's core, *J. Geophys. Res.*, *119*, 4164–4177, doi:10.1002/2014JB010980.

Laio, A., S. Bernard, G. L. Chiarotti, S. Scandolo, and E. Tosatti (2000), Physics of iron at Earth's core conditions, *Science*, *287*, 1027–1030, doi:10.1126/science.287.5455.1027.

Lay, T., J. Hernlund, and B. A. Buffett (2008), Core–mantle boundary heat flow, *Nature Geosci.*, *1*, 25–32, doi:10.1038/ngeo.2007.44.

Lister, J. R., and B. A. Buffett (1995), The strength and efficiency of thermal and compositional convection in the geodynamo, *Phys. Earth Planet. Inter.*, *91*, 17–30, doi:10.1016/0031-9201(95)03042-U.

Lord, O. T., M. J. Walter, R. Dasgupta, D. Walker, and S. M. Clark (2009), Melting in the Fe–C system to 70 GPa, *Earth Planet. Sci. Lett.*, *284*, 157–167, doi:10.1016/j.epsl.2009.04.017.

Lord, O. T., I. G. Wood, D. P. Dobson, L. Vočadlo, W. Wang, A. R. Thomson, E. T. H. Wann, G. Morard, M. Mezouar, and M. J. Walter (2014a), The melting curve of Ni to 1 Mbar, *Earth Planet. Sci. Lett.*, *408*, 226–236, doi:10.1016/j.epsl.2014.09.046.

Lord, O. T., E. T. H. Wann, S. A. Hunt, A. M. Walker, J. Santangeli, M. J. Walter, D. P. Dobson, I. G. Wood, L. Vočadlo, G. Morard, and M. Mezouar (2014b), The NiSi melting curve to 70 GPa, *Phys. Earth Planet. Inter.*, *233*, 13–23, doi:10.1016/j.pepi.2014.05.005.

Ma, Y., M. Somayazulu, G. Shen, H.-k. Mao, J. Shu, and R. J. Hemley (2004), In situ X-ray diffraction studies of iron to Earth-core conditions, *Phys. Earth Planet. Inter., 143–144*, 455–467, doi:10.1016/j.pepi.2003.06.005.

Morard, G., D. Andrault, N. Guignot, C. Sanloup, M. Mezouar, S. Petitgirard, and G. Fiquet (2008), *In situ* determination of Fe–Fe_3S phase diagram and liquid structural properties up to 65 GPa, *Earth Planet. Sci. Lett.*, *272*, 620–626, doi:10.1016/j.epsl.2008.05.028.

Morard, G., D. Andrault, N. Guignot, J. Siebert, G. Garbarino, and D. Antonangeli (2011), Melting of Fe–Ni–Si and Fe–Ni–S alloys at megabar pressures: Implications for the core–mantle boundary temperature, *Phys. Chem. Minerals*, *38*, 767–776, doi:10.1007/s00269-011-0449-9.

Nguyen, J. H., and N. C. Holmes (2004), Melting of iron at the physical conditions of the Earth's core, *Nature*, *427*, 339–342, doi:10.1038/nature02248.

Nomura, R., K. Hirose, K. Uesugi, Y. Ohishi, A. Tsuchiyama, A. Miyake, and Y. Ueno (2014), Low core-mantle boundary temperature inferred from the solidus of pyrolite, *Science*, *343*, 522–525, doi:10.1126/science.1248186.

Ozawa, H., F. Takahashi, K. Hirose, Y. Ohishi, and N. Hirao (2011), Phase transition of FeO and stratification in Earth's outer core, *Science*, *334*, 792–794, doi:10.1126/science.1208265.

Ozawa, H., K. Hirose, T. Suzuki, Y. Ohishi, and N. Hirao (2013), Decomposition of Fe_3S above 250 GPa, *Geophys. Res. Lett.*, *40*, 4845–4849, doi:10.1002/grl.50946.

Poirier, J.-P. (1994), Light elements in the Earth's outer core: A critical review, *Phys. Earth Planet. Inter.*, *85*, 319–337, doi:10.1016/0031-9201(94)90120-1.

Pozzo, M., C. Davies, D. Gubbins, and D. Alfè (2012), Thermal and electrical conductivity of iron at Earth's core conditions, *Nature*, *485*, 355–358, doi:10.1038/nature11031.

Pozzo, M., C. Davies, D. Gubbins, and D. Alfè (2014), Thermal and electrical conductivity of solid iron and iron–silicon mixtures at Earth's core conditions, *Earth Planet. Sci. Lett.*, *393*, 159–164, doi:10.1016/j.epsl.2014.02.047.

Rohrbach, A., S. Ghosh, M. W. Schmidt, C. H. Wijbrans, and S. Klemme (2014), The stability of Fe–Ni carbides in the Earth's mantle: Evidence for a low Fe–Ni–C melt fraction in the deep mantle, *Earth Planet. Sci. Lett.*, *388*, 211–221, doi:10.1016/j.epsl.2013.12.007.

Rost, S., E. J. Garnero, Q. Williams, and M. Manga (2005), Seismological constraints on a possible plume root at the core–mantle boundary, *Nature*, *435*, 666–669, doi:10.1038/nature03620.

Sakamaki, K., E. Takahashi, Y. Nakajima, Y. Nishihara, K. Funakoshi, T. Suzuki, and Y. Fukai (2009), Melting phase relation of FeH*x* up to 20 GPa: Implication for the temperature of the Earth's core, *Phys. Earth Planet. Inter.*, *174*, 192–201, doi:10.1016/j.pepi.2008.05.017.

Salamat, A., R. A. Fischer, R. Briggs, M. I. McMahon, and S. Petitgirard (2014), *In situ* synchrotron X-ray diffraction in the laser-heated diamond anvil cell: Melting phenomena and synthesis of new materials, Coord. *Chem. Rev., 277–278*, 15–30, doi:10.1016/j.ccr.2014.01.034.

Saxena, S. K., G. Shen, and P. Lazor (1994), Temperatures in Earth's core based on melting and phase transformation experiments on iron, *Science*, *264*, 405–407, doi:10.1126/science.264.5157.405.

Seagle, C. T., D. L. Heinz, A. J. Campbell, V. B. Prakapenka, and S. T. Wanless (2008), Melting and thermal expansion in the Fe–FeO system at high pressure, *Earth Planet. Sci. Lett.*, *265*, 655–665, doi:10.1016/j.epsl.2007.11.004.

Seagle, C. T., E. Cottrell, Y. Fei, D. R. Hummer, and V. B. Prakapenka (2013), Electrical and thermal transport properties of iron and iron–silicon alloy at high pressure, *Geophys. Res. Lett.*, *40*, 5377–5381, doi:10.1002/2013GL057930.

Shen, G., V. B. Prakapenka, M. L. Rivers, and S. R. Sutton (2004), Structure of liquid iron at pressures up to 58 GPa, *Phys. Rev. Lett.*, *92*, 185701, doi:10.1103/PhysRevLett.92.185701.

Sola, E., and D. Alfè (2009), Melting of iron under Earth's core conditions from diffusion Monte Carlo free energy calculations, *Phys. Rev. Lett.*, *103*, 078501, doi:10.1103/PhysRevLett.103.078501.

Stewart, A. J., M. W. Schmidt, W. van Westrenen, and C. Liebske (2007), Mars: A new core-crystallization regime, *Science*, *316*, 1323–1325, doi:10.1126/science.1140549.

Terasaki, H., S. Kamada, T. Sakai, E. Ohtani, N. Hirao, and Y. Ohishi (2011), Liquidus and solidus temperatures of a Fe–O–S alloy up to the pressures of the outer core: Implication for the thermal structure of the Earth's core, *Earth Planet. Sci. Lett.*, *304*, 559–564, doi:10.1016/j.epsl.2011.02.041.

Urakawa, S., M. Kato, and M. Kumazawa (1987), Experimental study on the phase relations in the system Fe–Ni–O–S up to 15 GPa, in *High-Pressure Research in Mineral Physics*, edited by M. H. Manghnani and Y. Syono, pp. 95–111, Terra Scientific Pub., Tokyo, and AGU, Washington, D.C.

Williams, Q., R. Jeanloz, J. Bass, B. Svedsen, and T. J. Ahrens (1987), The melting curve of iron to 250 gigapascals: A constraint on the temperature at Earth's center, *Science*, *236*, 181–182, doi:10.1126/science.236.4798.181.

Yamazaki, D., E. Ito, T. Yoshino, A. Yoneda, X. Guo, B. Zhang, W. Sun, A. Shimojuku, N. Tsujino, T. Kunimoto, Y. Higo, and K.-i. Funakoshi (2012), *P-V-T* equation of state for ϵ-iron up to 80 GPa and 1900 K using the Kawai-type high pressure apparatus equipped with sintered diamond anvils, *Geophys. Res. Lett.*, *39*, L20308, doi:10.1029/2012GL053540.

Yoo, C. S., N. C. Holmes, M. Ross, D. J. Webb, and C. Pike (1993), Shock temperatures and melting of iron at Earth core conditions, *Phys. Rev. Lett.*, *70*, 3931–3934, doi:10.1103/PhysRevLett.70.3931.

Zhang, L., and Y. Fei (2008), Effect of Ni on Fe–FeS phase relations at high pressure and high temperature, *Earth Planet. Sci. Lett.*, *268*, 212–218, doi:10.1016/j.epsl.2008.01.028.

Zhang, Y., T. Sekine, H. He, Y. Yu, F. Liu, and M. Zhang (2014), Shock compression on Fe–Ni–Si system to 280 GPa: Implications for the composition of the Earth's outer core, *Geophys. Res. Lett.*, *41*, 4554–4559, doi:10.1002/2014GL060670.